Differential synaptic processing separates stationary from transient inputs to the auditory cortex

Marco Atzori[1], Saobo Lei[1], D. Ieuan P. Evans[1], Patrick O. Kanold[2], Emily Phillips-Tansey[1], Orinthal McIntyre[1] and Chris J. McBain[1]

[1] *LCMN/NICHD/NIH, Rm 5A72, Bldg 49, Convent Drive, Bethesda, Maryland 20892-4495, USA*

[2] *Department of Biomedical Engineering, Johns Hopkins University, Baltimore, Maryland 21205, USA*

Correspondence should be addressed to C.J.McB. (chrismcb@codon.nih.gov)

Published online: 5 November 2001, DOI: 10.1038/nn760

Sound features are blended together *en route* to the central nervous system before being discriminated for further processing by the cortical synaptic network. The mechanisms underlying this synaptic processing, however, are largely unexplored. Intracortical processing of the auditory signal was investigated by simultaneously recording from pairs of connected principal neurons in layer II/III in slices from A1 auditory cortex. Physiological patterns of stimulation in the presynaptic cell revealed two populations of postsynaptic events that differed in mean amplitude, failure rate, kinetics and short-term plasticity. In contrast, transmission between layer II/III pyramidal neurons in barrel cortex were uniformly of large amplitude and high success (release) probability (P_r). These unique features of auditory cortical transmission may provide two distinct mechanisms for discerning and separating transient from stationary features of the auditory signal at an early stage of cortical processing.

Sensory cortices perform sophisticated pattern recognition tasks, elaborating the thalamic input via a variety of functionally different synapses across the six layers. The role of the auditory cortex in processing and modifying auditory signals, however, is largely unknown. Thalamic inputs to primary auditory cortex (A1) show several types of responses to acoustic stimuli, which fall into two broad classes of 'transient' and 'sustained' firing patterns[1–3]. Sustained responses saturate and can even be inhibited at increasing sound pressure level (SPL), whereas transient responses do not saturate or decrease at increasing SPL, suggesting differential mechanisms of synaptic processing. How these afferent signals are processed by downstream elements is unknown and may rely on distinct intrinsic conductances, synaptic inputs, ensemble coding or a combination of these or other factors.

Neurons within layer II/III of the auditory cortex receive direct thalamic input in addition to inputs from both layer IV spiny stellate neurons and other layer II/III neurons[4–6]. Output from layer II/III pyramidal neurons project to local layer V and layer II/III in neighboring and contralateral cortical areas, feeding all subsequent stages of auditory signal analysis. Anatomical studies have identified pyramidal cells in layer II/III of the auditory cortex with different types of axonal recurrent collateral patterns[4,5,7] raising the possibility of differential functional interactions within auditory columns[8]. We wanted to test the hypothesis that such intrinsic connections had the potential for functionally differentiating between either transient or sustained firing patterns. Here we demonstrate the existence of two modes of transmission between pyramidal neurons of layer II/III of the auditory cortex using paired whole-cell recordings. These two modes of transmission differed with respect to their success probability, EPSC amplitude, kinetics and short-term plasticity. In contrast, identical experiments done between layer II/III pyramidal cells in barrel cortex reveal a uniformly homogeneous population of connections with large amplitude EPSCs and high release probability, indicating that the properties of layer II/III auditory cortex connections do not represent two populations of connections common to other sensory cortical areas. We propose that these two synaptic networks implement two spectrally different tasks: the low probability synapses support ensemble-encoded narrow-band, long-lasting input, and the high probability synapses serve as reliable event detectors and wide-band signal analyzers.

Results

We recorded from over 100 pairs of layer II/III pyramidal neurons, which resulted in 37 synaptic connections in 35 pairs (two were reciprocally connected). All recordings were made at room temperature (~22°C) with the presynaptic cell held under current clamp and postsynaptic cell held under voltage clamp. Synaptic currents evoked by single action potentials in the presynaptic cell (stimulus frequency, 0.06 Hz) were blocked by the AMPA receptor antagonist DNQX (10 μM, $n = 6$), confirming that connections were glutamatergic in nature. Synaptic events were insensitive to exogenous application of philanthotoxin (2 μM, $n = 11$, data not shown), indicating that synapses contained predominantly GluR2-containing, Ca^{2+}-impermeable AMPA receptors[9–14].

In 24 of 37 connections, transmission occurred with a low probability ('weak connections'), with most presynaptic action potentials failing to produce detectable postsynaptic events (**Figs. 1a** and **2a**). The remaining 13 connections demonstrated synaptic transmission with a higher success probability with

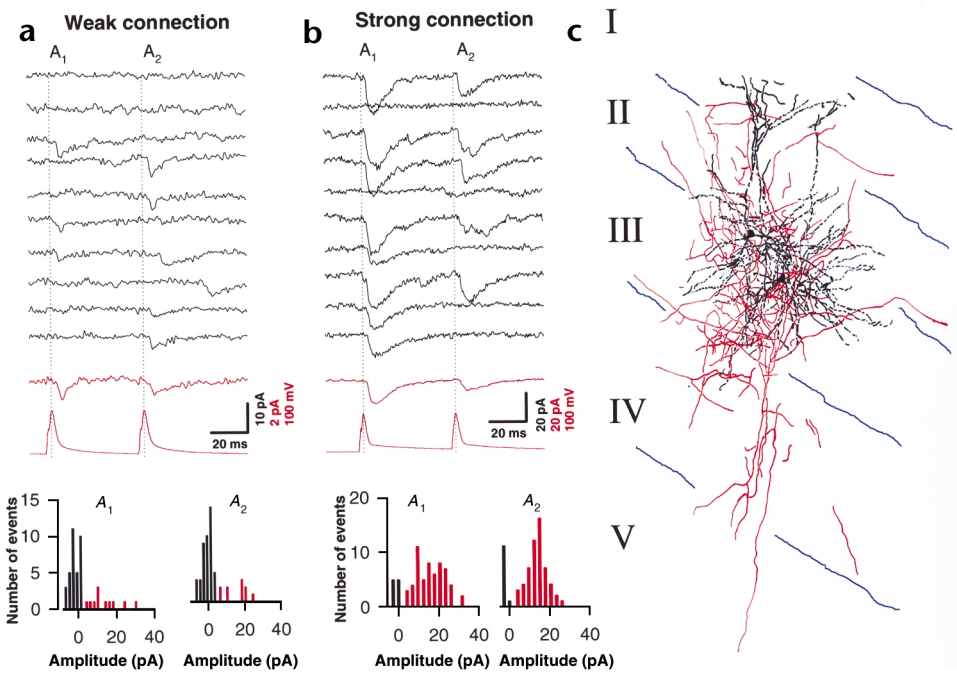

Fig. 1. Two layer II/III cortico–cortical excitatory connection phenotypes. (**a**) Representative example of a 'weak connection' synapse. Top, single traces showing EPSCs evoked by paired-pulse stimulation (stimuli separated by 50 ms). Average (n = 50) EPSCs and presynaptic spikes are in red. Bottom, amplitude histograms from 50 trials for the first and second synaptic responses. Synaptic failures and events are reported in black and red, respectively. (**b**) Representative example of a 'strong connection' synapse. Setup for figure is the same as for (**a**). Note scale differences between (**a**) and (**b**). Bottom, EPSC amplitude histograms from 70 trials. (**c**) Camera lucida drawing of the corresponding neurons used in panel (**b**). Cell bodies were located within layer III, whereas dendrites (black) projected deep into layers I–IV. The axon (indicated in red) made many local collaterals before projecting to layer V.

only a small number of failures of transmission ('strong connections'; **Figs. 1b** and **2a**).

A plot of the probability of transmission success ($P_r = 1$ – failures) between all connections revealed a histogram composed of two distinct clusters (**Fig. 2a**). One cluster, which we defined as 'low-probability connections' (LPCs), had P_r values less than 0.4 (mean ± s.e.m., 0.13 ± 0.02). We defined the second cluster, which had P_r values greater than 0.5 (mean ± s.e.m., 0.68 ± 0.02), as 'high probability connections' (HPCs). To determine whether the P_r dataset (**Fig. 2a**) represented a single population with a broad P_r distribution, data were fit with homogeneous, single Gaussian and single Poissonian distributions. None of these fits gave acceptable χ^2 values. In contrast, when the dataset were fit by the sum of two Gaussians or the sum of two first-order Poissonian dis-

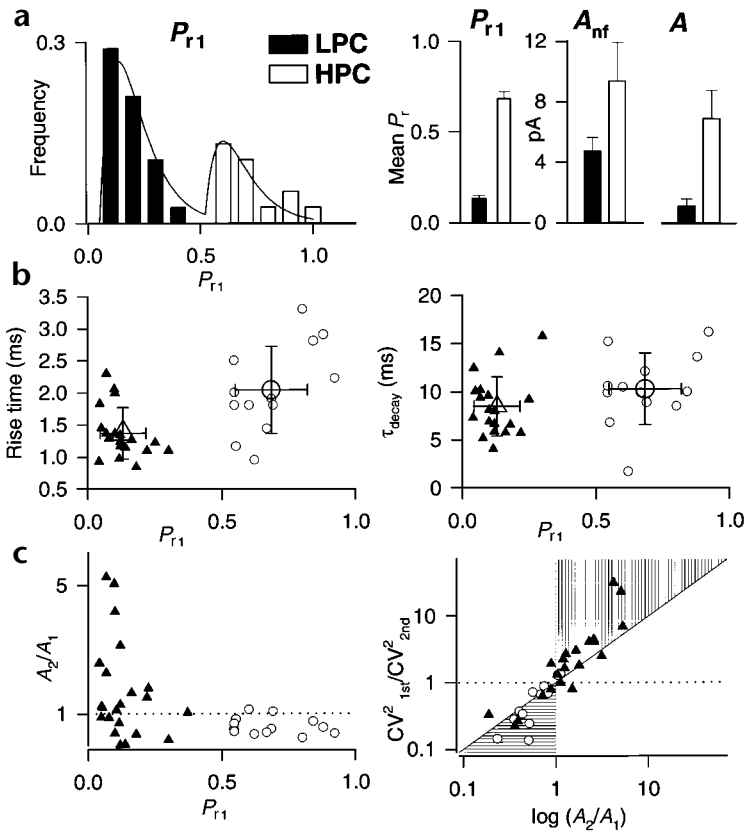

Fig. 2. Differing properties of HPCs and LPCs. (**a**) Left, histogram plots of release probability (P_{r1}) for synaptic responses in all connections (n = 37). The discontinuous distribution reveals two modes of transmission, one with low probability and one with high probability (24/37 and 13/37 connections, respectively). The largest population comprised those with a high initial release probability (HPC, open columns), with mean success probability (P_r) of 0.68 (right). The second class, low probability connections (LPC, black columns) had a mean probability across connections of 0.13. The P_r distribution was best fit by the sum of two Poissonian distributions (continuous line). Right three panels, mean values for the release probability, EPSC amplitudes measured in the absence of event failures (A_{nf}) and total EPSC amplitude (A, measurement including failures) of the two groups. (**b**) 10–90% rise time (left) and decay time constant (τ, right) versus P_{r1}. Individual experiments are shown by small symbols. The mean values across all data are indicated by large symbols. LPC, triangles; HPC, circles. (**c**) Left, paired-pulse ratio A_2/A_1 versus success probability of the first EPSC. All but two HPCs demonstrated paired-pulse depression, whereas LPCs could show either depression or facilitation. Right, CV^2 analysis suggests that presynaptic mechanisms (indicated by hatched areas) largely determine the response to paired-pulse stimuli. In this figure, error bars represent standard deviation to allow better resolution of the data scatter.

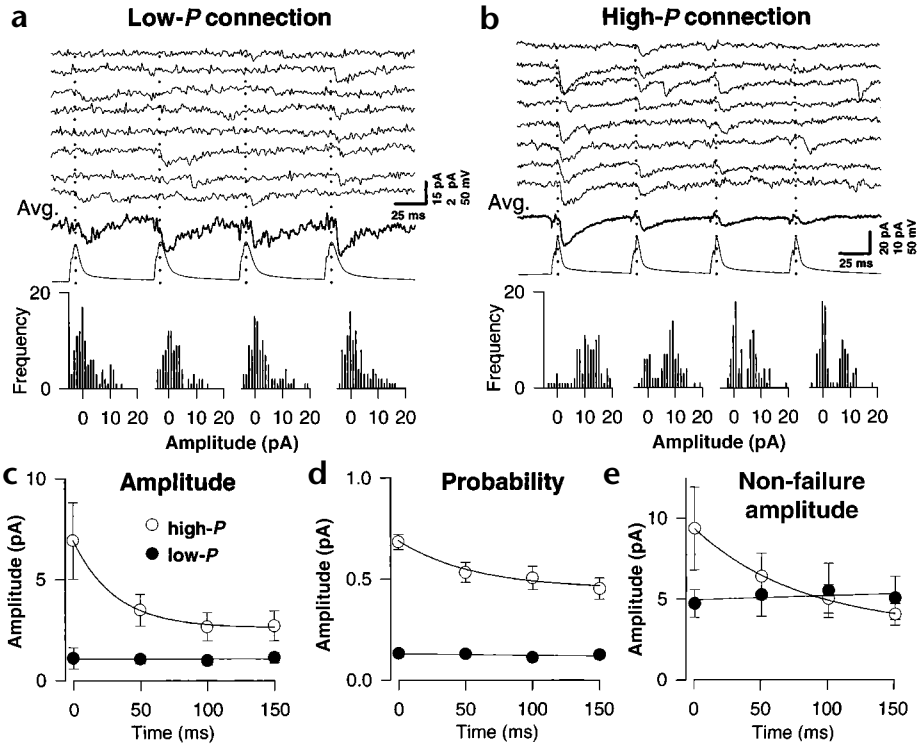

Fig. 3. Short-term plasticity at LFCs and HFC connections. High- and low-*P* connections demonstrate significantly different modes of short-term plasticity in response to trains of action potentials. Eight representative individual records in response to 20-Hz trains of presynaptic action potentials (lower traces) in LPCs (**a**) and HPCs (**b**). The mean response is shown below in bold for both types of connections. Amplitude histograms for each of the four synaptic responses in the spike train (n = 100 events for each histogram for both the LPC and the HPC) are shown below the individual traces. LPCs had smaller but stationary amplitudes during the course of the stimulus train. In contrast, HPCs possessed a larger amplitude response whose mean amplitude shifted to lower values as the train progressed. The number of failures increased during the stimulus train. (**c–e**) Average EPSC amplitude, probability and non-failure amplitude for all connections within the two groups (n = 13 for HPCs and n = 24 for LPCs). Whereas the HPCs showed a reduction in mean amplitude, probability and non-failure amplitude during the spike train, LPC parameters were constant throughout the stimulus train. Solid lines are single exponential fits of the experimental data. The numeric values for τ are 31 ± 4 ms, 56 ± 28 ms, and 80 ± 11 ms for (**c**), (**d**) and (**e**), respectively.

tributions, the χ^2 values (5.7 and 0.8, respectively) were well within the $\chi^2_{0.05}$ range (<11.1 and <14.1, respectively). This suggests that the data do not represent an evenly distributed single population of synaptic connections, but rather, indicate that HPC and LPCs reflect synapses with two distinct modes of transmission between layer II/III pyramidal neurons. Throughout the remainder of this report, all data were obtained from 24 cell pairs for LPCs and 13 cell pairs for HPCs, unless specified otherwise.

Biophysical and paired-pulse properties

We next wanted to determine whether LPCs and HPCs differed in properties other than their release probability. We observed no obvious differences in the resting membrane potentials (LPCs, V_r = –59.6 ± 1.5 mV; HPCs, –61.3 ± 1.6 mV), input resistance of the postsynaptic cells (LPCs, R_{input} = 228 ± 38 MΩ, n = 11; HPCs, 243 ± 53 MΩ, n = 6), or latency of EPSC onset (LPCs, mean latency, 2.9 ± 0.3 ms, n = 19; HPCs, 2.3 ± 0.2, n = 11). Analysis of EPSC kinetics revealed that the 10–90% rise time differed between the two populations (LPCs, 1.5 ± 0.2 ms, n = 19; HPCs, 2.0 ± 0.3 ms, n = 13, $p < 0.01$) but not the decay time constant (LPCs, 8.4 ± 0.7 ms, n = 19; HPCs, 10.3 ± 1.1 ms, n = 13, p = 0.16; **Fig. 2b**). We also observed significant differences between the mean EPSC amplitudes including failures (LPCs, A = 1.1 ± 0.5 pA; HPCs, A = 6.9 ± 1.9 pA) and excluding failures (LPCs, $EPSC_{nf}$ = 4.7 ± 0.9 pA, n = 22; HPCs, 9.3 ± 2.6 pA, n = 13, p = 0.046; **Fig. 2a**).

We next determined whether the paired-pulse ratio (PPR) of synaptic transmission in response to two closely time action potentials (50 ms) in the presynaptic cell were similar for LPCs and HPCs. At LPCs, the amplitude of the second EPSC demonstrated either facilitation or depression in response to paired-pulse stimuli. The paired-pulse ratio (PPR) from all connections ranged from 0.18 to 5.3 (**Fig. 2c**). However, across all recordings, the mean amplitude of the second EPSC was not significantly different from the first EPSC amplitude ($EPSC_1$ = 1.1 ± 0.5 pA; $EPSC_2$ = 1.1 ± 0.2 pA). In contrast, all but two of the HPCs displayed strong depression ($EPSC_1$ = 6.9 ± 1.9 pA; $EPSC_2$ = 3.5 ± 0.8 pA; **Fig. 2c**), with a mean PPR in the range of 0.23–1.13. The ratio P_{r2}/P_{r1} ($P_{r1,2}$, success probability of the first and second EPSC) also differed between the two connection types: P_{r2}/P_{r1} was 1.28 ± 0.17 for LPCs, and 0.78 ± 0.06 for HPCs. Evidence that presynaptic mechanisms determine the observed response to paired-pulse stimuli in both LPCs and HPCs was suggested by CV^2 (amplitude mean/variance) analysis[16] (**Fig. 2c**).

We next determined whether any of the measured parameters, P_r, EPSC amplitude, $EPSC_{nf}$ or the paired pulse ratio, were correlated with the developmental age range used throughout our experiments (postnatal day 18–28). None of these parameters were correlated with the postnatal age of animals (P_r versus age, r = 0.16; mean amplitude, r = 0.31; $EPSC_{nf}$, r = 0.3; paired-pulse ratio, r = –0.09; data not shown). Similarly, no correlation existed between the intersomatic distances between the pairs of layer II/III pyramidal cells chosen for study (intersomatic distances measured from *post hoc* anatomical analysis) and the P_r (r = 0.04).

Short-term plasticity in response to spike trains

Units in A1 recorded *in vivo* have an upper firing frequency limit between 40 and 60 Hz[17], and cortical integration times are of the order of 20–150 ms[18]. Moreover, *in vivo* cortical units respond to repeated auditory stimuli up to frequencies of about 20 Hz[19]. Therefore, trains of spikes 150 ms long at 20 Hz (repeated 30–150 times at 15-second intervals, to allow complete recovery from depression or facilitation) were selected to simulate physiological stimuli. The postsynaptic response to the presynaptic spike train markedly dif-

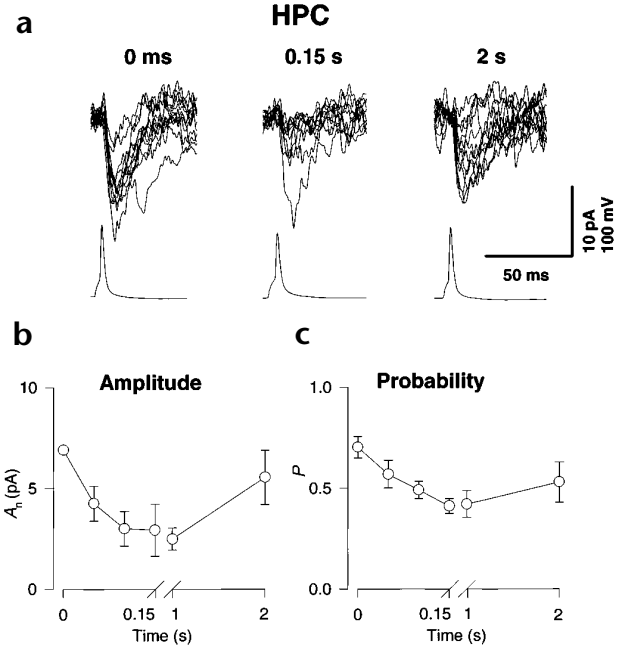

fered between LPCs and HPCs. On average, LPCs displayed no change in mean amplitude, P_r or $EPSC_{nf}$ of any EPSCs occurring during the train (**Fig. 3a, c–e**). In contrast, HPCs displayed depression of all three parameters when comparing the fourth to the first event in the train (**Fig. 3b–e**). In all cases, the observed amplitude (or probability) depression was best described by a single exponential function (**Fig. 3c–e**). Despite the observation of significant short-term depression of transmission during trains of stimuli at HFCs, the mean EPSC amplitude remained significantly greater than that of the corresponding LFCs (**Fig. 3c**). The mean value of the fourth EPSC was 1.1 ± 0.2 pA for LPCs, and 2.7 ± 0.7 pA for HPCs. Similarly, despite the decrease in P_r during successive events in the train, P_{r4} (success probability of the fourth response) in HPCs remained significantly higher than that of the LPCs (HPCs, P_{r4} = 0.5 ± 0.1; LPCs, 0.1 ± 0.2; **Fig. 3d**). The stable response of LPCs is qualitatively different from the depressing response observed in HPCs, and suggests that HPCs are not simply the numerical summation of multiple LPCs and that each represents a distinct mode of transmission between auditory cortex pyramidal cells.

Fig. 5. Differential dependence of short-term plasticity on $[Ca^{2+}]_o$ in HPCs. (**a–d**) Representative experiment demonstrating the effect of reducing $[Ca^{2+}]_o$ on short-term plastic properties. (**e**, **f**) Mean data from five experiments at high-probability connections. (**a–d**) Lowering $[Ca^{2+}]_o$ from 1.5 to 0.5 mM decreased both the mean amplitude and the success probability of EPSCs occurring early in the train. In contrast, the amplitudes of synaptic responses occurring later in the train were not significantly different from those recorded in 1.5 mM $[Ca^{2+}]_o$ (mean change in $EPSC_4$ amplitude, 5 ± 2%). (**c**, **e**) This redistribution of EPSC amplitude acts to minimize the short-term depression observed in control $[Ca^{2+}]_o$. The influence of $[Ca^{2+}]_o$ on short-term plasticity is more clearly observed when the two data sets are normalized to their respective first EPSC amplitudes (**e**, inset), which clearly illustrates that the depressing response of HPCs in control $[Ca^{2+}]_o$ is converted to a 'stationary' response in low $[Ca^{2+}]_o$. (**d**) A comparison of the P_r in the two $[Ca^{2+}]_o$ conditions suggests that a reduction of P_{r1} and P_{r2} contributes to the reduction of $EPSC_1$ and $EPSC_2$ amplitude observed in panel (**c**). (**f**) Examination of the mean P_r data reveals that in general, the largest reduction in P_r was associated with P_{r1}.

Fig. 4. Time course of recovery from short-term depression at HPCs. To determine the time course of recovery from depression in HPCs, experiments similar to those shown in Fig. 4 were repeated, but the initial 20-Hz train was followed by stimuli 1 and 2 s after the termination of the train. (**a**) Example of HPC activity at 3 time points during the train and 2 s following termination of the train. Each panel represents 10 traces evoked by single action potentials (bottom). Left and middle traces represent the first and fourth events in the train and illustrate the significant depression of the event amplitude. Right, recovery of the event amplitude at a 2-s time point after termination of the train. (**b**, **c**) The mean time course of the recovery for the EPSC amplitude and probability, respectively (n = 6 connections).

Time course of recovery from short-term depression

To determine the time course of recovery from short-term depression in HPCs, experiments similar to those described above were repeated, but the initial 20 Hz train was then followed by stimuli 1–2 seconds after the train. In 6 HPCs (**Fig. 4**), the depression of the EPSC mean amplitude occurring during the 20-Hz conditioning train did not fully recover until about 2 seconds after termination of the 20-Hz spike train ($EPSC_1$ = 6.9 ± 0.8 pA, $EPSC_4$ = 2.9 ± 1.3 pA, $EPSC_{1second}$ = 2.5 ± 0.5 pA, $EPSC_{2seconds}$ = 5.5 ± 1.3 pA; **Fig. 4b** and **c**). The time course for amplitude recovery did not parallel that of the recovery of P_r (**Fig. 4c**) (mean P_rEPSC_1 = 0.70 ± 0.05, P_rEPSC_4 = 0.41 ± 0.04, $P_rEPSC_{1second}$ = 0.42 ± 0.07, $P_rEPSC_{2seconds}$ = 0.53 ± 0.10). These data suggest that two distinct mechanisms with distinct kinetics may underlie recovery from short-term depression.

$[Ca^{2+}]_o$-dependence of short-term plasticity

Several features of synaptic transmission, such as release probability and the degree of depression or facilitation in response to

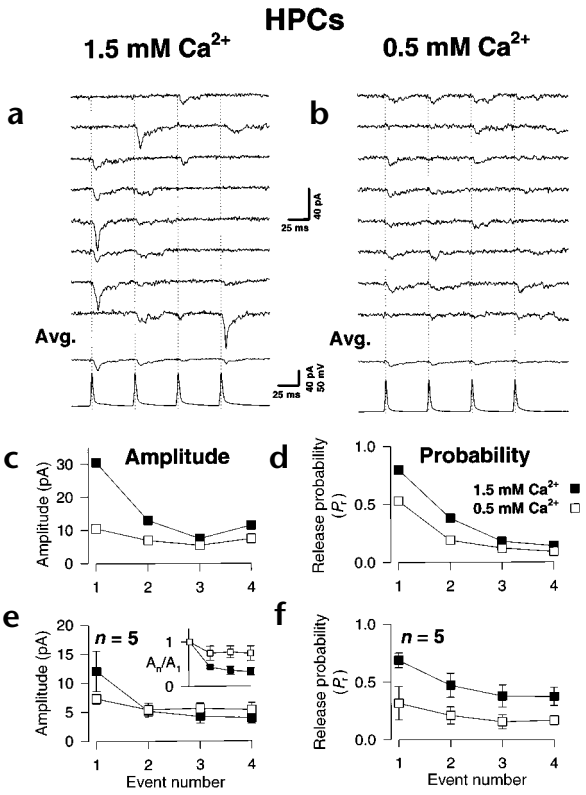

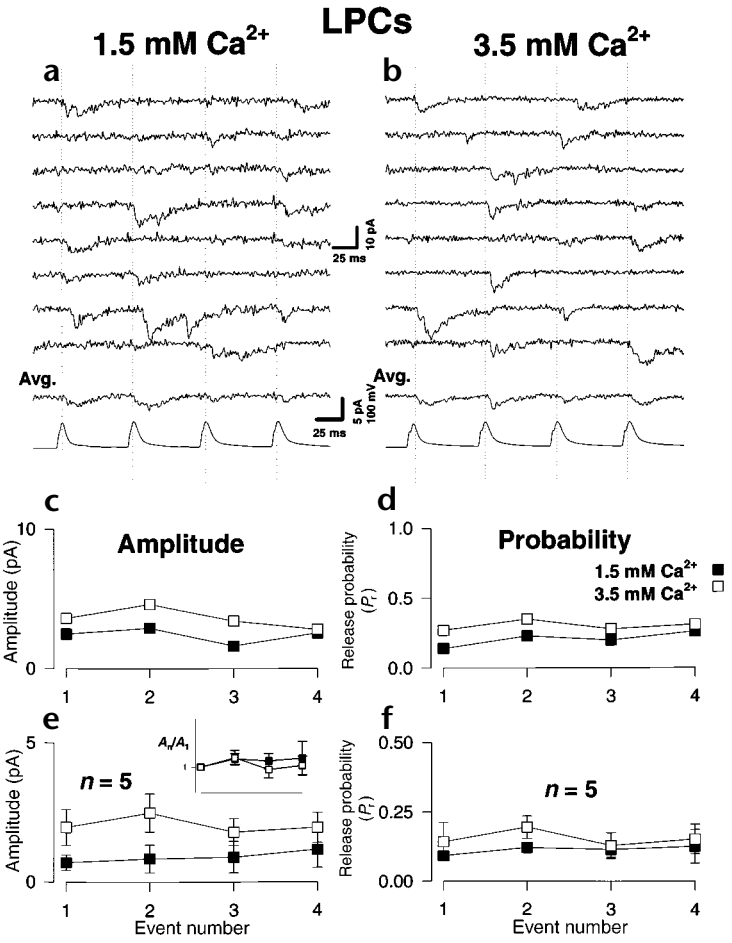

Fig. 6. Differential dependence of short term plasticity on $[Ca^{2+}]_o$ in LPCs. Greater than twofold elevation in $[Ca^{2+}]_o$ fails to convert the stationary response of LPC short-term plasticity into a depressing one. Figure setup is identical to Fig. 5. At LPC connections, an elevation of $[Ca^{2+}]_o$ from 1.5 to 3.5 mM results in an increase in the mean amplitude and P_r of EPSCs occurring early in the train (**c–f**). However, this increase in EPSC amplitude or P_r was not accompanied by any alteration of the short-term plastic properties of the synapse (**e**, inset).

trains of stimuli, are tightly regulated by the extracellular calcium ion concentration ($[Ca^{2+}]_o$)[20,21]. For example, at connections between hippocampal pyramidal neurons, the degree of paired-pulse depression increases with elevation of $[Ca^{2+}]_o$[22], indicating that short-term plasticity is strongly influenced by the initial presynaptic release probability. To determine whether the differential response to brief trains of stimuli of HPCs and LPCs resulted from differences in the initial P_r, we next examined the role of $[Ca^{2+}]_o$ in shaping the synaptic response to short trains of presynaptic activity. Specifically, we wanted to determine whether the pattern of short-term plasticity at HPCs could be converted to activity characteristic of LPCs by simply decreasing $[Ca^{2+}]_o$, and vice versa.

In 5 HPC recordings, $[Ca^{2+}]_o$ was decreased from 1.5 to 0.5 mM (whereas $[Mg^{2+}]_o$ was raised from 1.5 to 2.5 mM). Such a reduction in Ca^{2+} and elevation of Mg^{2+} allowed us to manipulate the amplitude and P_r of $EPSC_1$ to approximate LPCs. The reduction in $[Ca^{2+}]_o$ reduced the mean $EPSC_1$ amplitude by 40 ± 8% (**Fig. 5**), but had little effect on events occurring later in the train (mean change in $EPSC_4$ amplitude, 5 ± 2%; **Fig. 5c** and **e**). This redistribution of EPSC amplitude reduced the short-term depression observed in control $[Ca^{2+}]_o$: in low-$[Ca^{2+}]_o$, $EPSC_1$ and $EPSC_4$ amplitudes were not significantly different ($EPSC_1$ = 7.3 ± 0.8 pA versus $EPSC_4$ = 5.4 ± 1.2 pA, $p = 0.28$). The short-term plastic properties of HPCs in low $[Ca^{2+}]_o$ were similar to those observed at LPCs in 1.5 mM $[Ca^{2+}]_o$ (compare with **Fig. 3c**). This was more clearly illustrated when the two data sets were normalized to their first EPSC amplitudes (**Fig. 5e**, inset), which showed that a depressing response at HPCs is converted to a 'stationary' response in lowered $[Ca^{2+}]_o$.

Lowering $[Ca^{2+}]_o$ significantly reduces the P_r of $EPSC_1$ and $EPSC_2$ (**Fig. 5a** and **b**). This reduction of P_{r1} and P_{r2} likely contributed to the smaller $EPSC_1$ and $EPSC_2$ amplitude (**Fig. 5c**). Across all experiments, the largest reduction in P_r of all events in the train was associated with P_{r1} (mean $P_{r1low[Ca^{2+}]_o}$/mean $P_{r1ctrl[Ca^{2+}]_o}$ = 0.46 ± 0.15, **Fig. 5f**). This reduction in P_r of events early in the train endows HPC synapses with transmission properties reminiscent of LPCs.

In contrast, the pattern of short-term plasticity at LPCs was not altered by elevating $[Ca^{2+}]_o$. In 5 experiments, $[Ca^{2+}]_o$ was elevated from 1.5 to 3.5 mM (and $[Mg^{2+}]_o$ was decreased to 0.5 mM). Under these conditions, we observed an increase in the mean amplitude and P_r of EPSCs occurring early in the train (**Fig. 6**; mean increase in $EPSC_1$ amplitude, 160 ± 98% of control). However, this increase in EPSC amplitude did not alter the pattern of short-term plasticity at these synapses (that is, we were unable to convert a 'stationary' response to a 'depressing' one; **Fig. 6c** and **e** and inset, compare **Fig. 5c** and **e**). Indeed, on no occasion did we observe a LPC that demonstrated HPC-like short-term plasticity in elevated $[Ca^{2+}]_o$ conditions. These data suggest that although transmission in LPCs is sensitive to changes in $[Ca^{2+}]_o$, LPCs could not be 'converted' to HPCs by simply changing their P_r.

Equivalent transmission is not observed in barrel cortex

To determine whether LPCs and HPCs were a general property of synapses between layer II/III pyramidal neurons in other sensory cortical areas, similar recordings were made from pyramidal neurons in barrel cortex slices[23] across an identical age range. Synaptic transmission between connected pairs of layer II/III pyramidal neurons from barrel cortex possessed properties fundamentally different from equivalent neurons in auditory cortex (**Fig. 7**). From a total of 18 connected pairs, the mean EPSC amplitude in response to single presynaptic stimulation was 19.6 ± 1.8 pA ($n = 18$), almost 3 times greater than the mean amplitude of connections between HPC in auditory cortex and about 20 times greater than LPC amplitudes (compare **Figs. 1** and **2**). The probability of synaptic transmission was also significantly higher at barrel cortex connections (mean $P_r = 0.93 \pm 0.01$, $n = 18$; **Fig. 7e**) with few failures of synaptic transmission occurring (**Fig. 7a**, **b**, **d**; compare with HPC mean $P_r = 0.68$). Consequently, the mean EPSC amplitude, excluding failures (mean, 20.9 ± 1.9 pA) was significantly greater than observed in either auditory cortex HPC (9.3 pA) or LPC (4.7 pA).

Responses to short trains of presynaptic stimuli were invariably depressing (**Fig. 7**) with the mean EPSC amplitude, mean EPSC amplitude excluding failures and P_r all showing signifi-

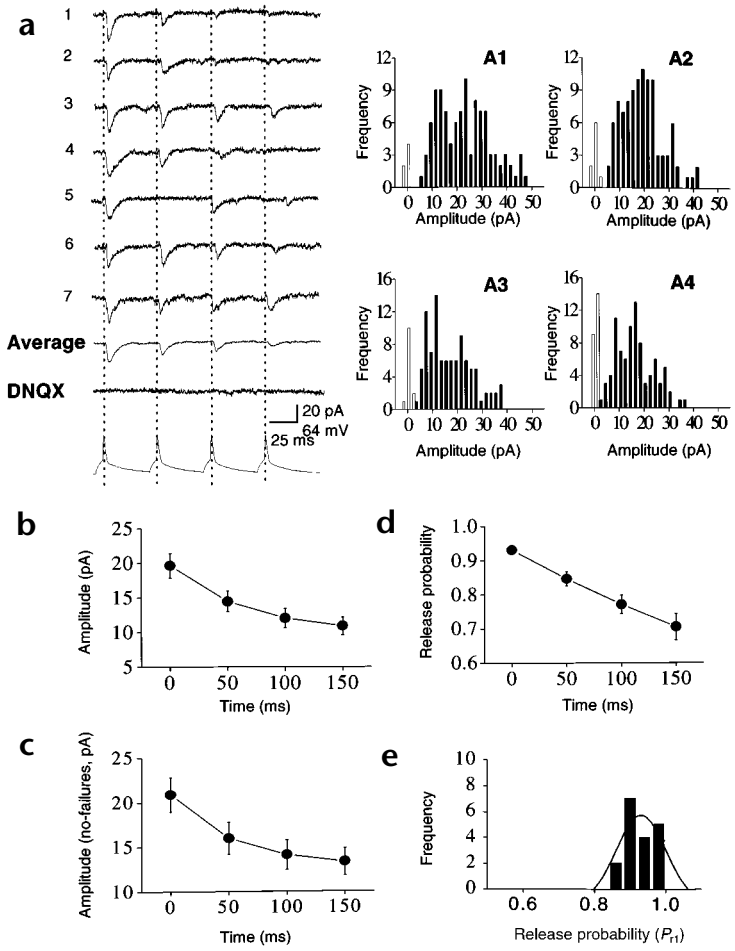

Fig. 7. Equivalent connections were not observed in barrel cortex. Experiments identical to those illustrated in Fig. 3 were made between pairs of connected neurons recorded from layer II/III pyramidal neurons in barrel cortex. (**a**) Representative single experiment and panels (**b–d**) illustrate the mean pooled data from 18 connected pairs. (**a–c**) In all cases, connections between layer II/III pyramidal neurons possessed large EPSC amplitudes far in excess of those observed in the layer II/III auditory connection. (**a**) Seven sample traces of synaptic activity in response to trains of 20-Hz presynaptic action potentials (bottom). An average of 30 traces (third from bottom) illustrates that this connection possessed short-term depression in response to the 20-Hz train. In the presence of the AMPA receptor antagonist, DNQX, all transmission was blocked, indicating the glutamatergic nature of this connection. Right, amplitude histograms constructed from cell shown on left. Failures are indicated by open columns and successes by solid columns. (**b–e**) Mean data from 18 connections. In all cases, the EPSC amplitude (**b**) and EPSC amplitude excluding failures (**c**) showed strong depression in response to the train of 20-Hz stimuli. (**d**, **e**) The mean initial release probability of connections in barrel cortex was extremely high, with little evidence for synaptic failures (compare with **Figs. 1–3**). The mean P_r decreased during the train of presynaptic stimuli. (**e**) Distribution of P_{r1} from all 18 connections show that all connections possess a uniformly high P_{r1}. Solid line is fit by single Gaussian function.

cant depression during the 20-Hz train of stimuli (**Fig. 7b–d**). Despite demonstrating significant reduction in the mean P_r during the course of the stimulus train ($P_{r1} = 0.93 \pm 0.01$ versus $P_{r4} = 0.70 \pm 0.03$, $n = 18$), P_{r4} was still significantly greater in barrel cortex that P_{r4} in HPC auditory cortex (~0.5). Similarly, the mean value of the $EPSC_4$ was 10.9 ± 1.3 pA ($n = 18$) in barrel cortex compared to 1.1 pA and 2.7 pA for LPC and HPC in auditory cortex. Taken together, these data demonstrate that connections between layer II/III pyramidal neurons in barrel cortex possess properties distinct from those observed in auditory cortex. Moreover, these data suggest that HPC and LPCs do not represent a homogeneous property of synaptic connections common to other sensory cortical areas.

A high level of connectivity within layer II/III

In recordings from auditory cortex, spontaneous excitatory synaptic activity often occurred synchronously on both the presynaptic and postsynaptic neuron, suggesting that common sources may innervate layer II/III neurons. We next determined whether the incidence of such synchronous synaptic activity preferentially occurred on pairs of cells that were connected by LPC or HPCs compared to pairs of cells that were not synaptically connected.

Correlated spontaneous EPSCs were detected primarily in recordings from connected cells (**Fig. 8**). The synchronous nature of spontaneous events detected in cell pairs was confirmed by the presence of a sharp peak in cross-correlograms (**Fig. 8c**). The percentage of cells displaying synchronous spontaneous currents was higher in connected cells compared to non-connected cells, with the incidence of synchronous events being similar in LPCs (58%) and HPCs (64%). In contrast, only 18% of non-connected pairs received synchronous spontaneous synaptic activity (**Fig. 8d**). These data suggest the existence of synaptically connected ensembles whose components may be activated in concert[24].

Discussion

Here we provide functional evidence, based on differences in EPSC amplitude, success probability, kinetics and response to brief trains of stimuli, for two different modes of transmission between excitatory connections of the primary auditory cortex[7]. The most frequently observed transmission mode, the LPC, was associated with small mean EPSC amplitude, a low event success probability, and on average, a non-decremental response to 20-Hz spike trains. Transmission via HPCs was characterized by a high P_r, a larger mean EPSC amplitude, paired-pulse depression, and marked short-term depression in response to 20-Hz spike trains.

The differential response of LPCs and HPCs to short trains of presynaptic stimuli represented the most significant difference between the two modes of transmission. At LPCs, the mean EPSC amplitude and P_r remained constant at each successive event in the train. In contrast, both mean event amplitude and P_r decreased during the 20-Hz train at HPCs. This suggests that whereas the release machinery at LPCs can faithfully support brief trains of presynaptic stimuli, the decrease in both EPSC amplitude and P_r at HPCs favors their involvement in transient episodes. It is uncertain at this time whether LPCs and HPCs represent two distinct classes of connection or represent the extreme ends of a continuum ranging from low- to high-probability connections. Because a uniform distribution for P_r between cortical pyramidal neurons in layer V was reported previously[15], we considered the possibility that the clustering of LPCs and HPCs resulted from the finite sample size ($n = 37$). We considered this unlikely; were the data from a single population of connections, possessing a uniform

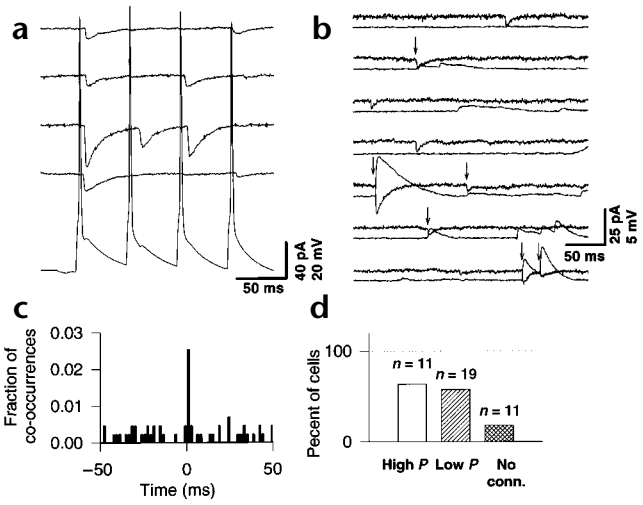

Fig. 8. Synchronous spontaneous synaptic input onto connected layer II/III cells. (**a**) An example of two connected cells (LPC-type). Lower traces indicate presynaptic action potentials; upper traces represent four representative trains of postsynaptic EPSCs. (**b**) The same two cells display numerous synchronous spontaneous EPSPs (upward deflections)/EPSCs (downward deflections) that originate from unidentified sources (indicated by arrows). (**c**) A zero lag in the cross correlation analysis confirms the synchronous nature of the co-occurring synaptic events. (**d**) Summary histogram showing that the fraction of cells showing simultaneous spontaneous EPSC is high in both HPCs and LPC connected pairs but lower in recordings of two cells showing no connectivity.

distribution of P_r, the probability of observing such a gap in the dataset within a single population would be extremely low ($p < 0.0001$). In addition, P_r frequency histograms (**Fig. 2a**) were well fit by the sum of two first-order Poissonian distributions but poorly fit by either a single Poissonian or Gaussian distribution. Thus, we consider it likely that LPCs and HPCs represent specific populations of synapse types whose transmission properties are tuned for specific roles in auditory cortex. This is underscored by the experiments from equivalent connections in barrel cortex. Transmission between layer II/III pyramidal neurons in barrel cortex occurred via synapses that had high release probability (mean $P_r = 0.93$) and large EPSC amplitudes, and that invariably demonstrated short-term depression of both EPSC amplitude and P_r in response to brief trains of stimuli.

Physiological function of HPCs and LPCs

In vivo recordings from thalamus show that a limited number of firing patterns exist in response to sustained tones or repetitive clicks. The response to tone stimulation, measured as mean firing rate, is either sustained or transient in nature[2]. Similarly, the two most frequently encountered patterns, classified according to the response to series of clicks, are the so-called 'lockers' and 'special responders'[1]. 'Lockers' respond to clicks presented at a frequency of up to about 50 Hz, faithfully following the stimulus, whereas 'special responders' respond only to the onset of the stimulus train. How these two types of signal are integrated within auditory cortex is largely unknown. We speculate that two synaptic 'channels' composed of connections with temporal characteristics observed in the present experiments could faithfully convey to cortical neurons (which fire up to approximately 20 Hz[19]) information encoded in transient or sustained patterns of thalamic input.

Because of the distinct properties of short-term plasticity, we propose that LPCs and HPCs may subserve fundamentally different functions in the auditory network. Input to a set of LPCs could act to support 'locker' responses, ensuring fidelity of the cortical output. A cortical unit receiving a sustained train of action potentials from a sufficient number of LPCs could indeed produce a sustained noise-insensitive response by integration of ensemble-coded synaptic excitatory input. On the contrary, supra-threshold input through a set of HPCs would result in a transient, depressing response, largely independent of the duration of the input signal. Thus, the brief activation of a few HPCs may generate 'special responder' patterns in cortical units. Consequently, a unit that is postsynaptic to HPCs may be particularly suited for detecting variability in the timing of signal location and frequency. An alternative or complementary role of depressing synapses is the detection of subtle differences of frequency-modulated signals[25]. These interpretations do not rule out the involvement of additional mechanisms, such as local inhibition or non-local cortical interactions, commonly invoked to explain shaping of excitatory responses. Future experiments are aimed at determining the role of inhibitory neurons within the circuitry.

In conclusion, pyramidal cells within layer II/III of the auditory cortex process incoming presynaptic signals using two synaptic networks with unique computational features. HPCs and LPCs networks in layer II/III provide a compelling synaptic substrate for performing spectrally heterogeneous demands of auditory cortical analysis, such as event detection and sound fingerprinting[26], possibly related to the 'what and where' processing in the auditory pathway[27].

Methods

Auditory cortex slices. C57/BL6 male mice (18–28 days old) were anesthetized according to the NIH Animal Care and User Committee guidelines, and their brains were placed for 1–2 min in ice-cold saline solution composed of 130 mM NaCl, 3.5 mM KCl, 24 mM $NaHCO_3$, 1.25 mM NaH_2PO_4, 0.5 mM $CaCl_2$, 3.0 mM $MgCl_2$ and 10 mM glucose. After removal of the cerebellum, 250-μm-thick coronal slices from the first sixth of the caudal part of the brain, where the primary auditory area A1 lies, were cut at 0–4°C. Slices were then incubated at 32°C in the same solution until used for recordings. Slices were subsequently moved to a recording chamber and superfused with a solution as above except that $[Ca^{2+}]$ and $[Mg^{2+}]$ were both 1.5 mM and maintained at room temperature.

Barrel cortex slices. Coronal slices (400 μm) containing the posteromedial barrel subfield were prepared from C57/BL6 mice (P18–P28) using previously described methods[23]. Mice were anesthetized with forane and decapitated, and the brain was rapidly removed in ice-cold saline solution as described above. The posterior part of the left hemisphere was vertically trimmed away at 50 degrees relative to the midsagittal plane. The trimmed surface was then glued downward to the vibratome (Leica, Deerfield, Illinois) stage and slices were cut from the rostral pole of the right hemisphere parallel to the trimmed surface. The initial 4 slices (about 1600 μm) were discarded and the next 5 slices (about 2000 μm) containing the whisker barrels were saved for recording. The slices were incubated at 32°C in the recording solution for 30 min and then maintained at room temperature until use. The posteromedial barrel subfield was identified by the presence of three to four large barrel-like structures in layer IV, visible under transillumination. Individual pyramidal neurons located within layer II/III were selected for recording based on somata size and position.

Recording. For recording pairs of auditory cortical pyramidal neurons in layer II/III, cells were selected according to their position, dorsal to the ectosylvian region, and shape of their cell bodies. Whole-cell patch-clamp recordings were performed using Axopatch-1D amplifiers. Signals were filtered at 2 kHz and digitized at 10 kHz on a PC using a Digidata 1200 interface driven by pClamp8 (Axon Instruments, Foster City, California). The intracellular electrode solution was composed of 90 mM KGluconate,

12 mM KCl, 10 mM HEPES, 2 mM EGTA, 2.0 mM ATP.Na_2, 0.3 mM GTP.Na, 1.0 mM $MgCl_2$ and 0.5% biocytin. This solution was selected to provide a reversal potential of –60 mV for Cl^- to minimize the contribution of GABAergic IPSCs. After obtaining cell pairs, suprathreshold electrotonic current pulses (200–300 ms) were delivered in current clamp to allow determination of the neuronal firing pattern to provide tentative identification that cells were pyramidal in nature. In all cases, the presence of an 'accommodating' action potential firing pattern in response to depolarizing current injection (postsynaptic cell now held under current-clamp conditions) and *post hoc* cell identification following biocytin injection (example in **Fig. 1c**) confirmed that all weakly and strongly connected neuron pairs were between pyramidal neurons.

Excitatory synaptic currents were recorded by holding the presynaptic cell in current clamp and postsynaptic one in voltage clamp at a holding potential of –60 mV. Synaptic currents were evoked at 0.06 Hz by delivering current pulses (1–3 ms, 0.3–2.0 nA) to the presynaptic cell held under current clamp. In some experiments, trains of 4 action potentials were generated at 20 Hz, repeated at 15-s intervals (40–140 times; on average, trains were repeated 80 times). In experiments to determine the recovery from short-term depression, additional EPSCs were elicited at 1–2-s intervals commencing after the spike train.

Biocytin staining. Following all recordings, slices were immediately transferred to a 24-well plate and fixed in a solution containing 80 mM Na_2HPO_4, 80 mM NaH_2PO_4 and 3.5% paraformaldehyde. Biocytin staining was then processed using diaminobenzidine as chromogen, using a standard ABC kit (Vector Labs, Burlingame, California). A light cresyl violet Nissl counterstain was used to identify the cortical layers.

Data analysis. The input and series resistance of the postsynaptic cell was constantly monitored by delivering a –5-mV voltage command. Cells whose input or series resistance changed by more than 30% of the initial value were discarded. Lists of events and failures were created for each recorded cell and for each peak amplitude in the train using a semiautomatic algorithm setting a threshold of two standard deviations of the noise amplitude. To measure peak amplitudes, the mean of the amplitude of the failures, corresponding to the peak of the noise, was first subtracted from the event amplitude list.

Latencies were determined from the peak of the presynaptic spike to the zero crossing of the straight line that best fitted the rising phase of a sample of 10–20 EPSCs. The same sample was used to calculate rise times (10–90%). Decay time constants were determined using single exponential curve fitting routines. Mean and s.e.m. are reported throughout unless otherwise indicated. Data were considered significant if $p < 0.05$.

CV^2 analysis was used to predict the locus of short term synaptic plasticity[16]. A change is represented as a point in the potentiation–CV^2 ratio (π–ρ) graph.

$CV^2 \equiv \mu/\sigma^2$, where $\mu \equiv$ mean amplitude and $\sigma^2 \equiv$ amplitude variance
$\pi \equiv \mu_{after}/\mu_{before}$ and $\rho \equiv CV^2$ ratio $\equiv CV^2_{before}/CV^2_{after}$

A data point in the regions between the $\rho = \pi$ and the $\pi = 1$ straight lines (indicated by hatched area in **Fig. 2d**) corresponds to a presynaptic locus.

Acknowledgements

We thank D. Feldman for his assistance in preparing Barrel cortex slices and C. Trouth for cell reconstruction and camera lucida drawings of neurons. This work was supported by an Intramural Research award to C.McB.

Received 24 September; Accepted 16 October 2001

1. Rouiller, E., de Ribaupierre, Y., Toros-Morel, A. & de Ribaupierre, F. Neural coding of repetitive clicks in the medial geniculate body of the cat. *Hear. Res.* **5**, 81–100 (1981).
2. Phillips, D. P. & Kelly, J. B. Coding of tone-pulse amplitude by single neurons in auditory cortex of albino rat. *Hear. Res.* **37**, 269–280 (1989).
3. Clarey, J. C., Barone, P. & Imig, T. J. in *The Mammalian Auditory Pathway: Neurophysiology* (eds. Popper, A. N. & Fay, R. R.) 232–334 (Springer, New York, 1992).
4. Winer, J. A. The pyramidal neurons in layer III of cat primary auditory cortex (AI). *J. Comp. Neurol.* **229**, 476–496 (1984).
5. Winer, J. A. Structure of layer II in cat primary auditory cortex (AI). *J. Comp. Neurol.* **238**, 10–37 (1985).
6. Metherate, R. & Aramakis, V. B. Intrinsic electrophysiology of neurons in thalamorecipient layers of developing rat auditory cortex. *Dev. Brain Res.* **115**, 131–44 (1999).
7. Clarke, S., de Ribaupierre, F., Rouiller, E. M. & de Ribaupierre, Y. Several neuronal and axonal types form long intrinsic connections in the cat primary auditory cortical field (AI). *Anat. Embryol. (Berl.)* **188**, 117–138 (1993).
8. Shen, J. X., Xu, Z. M. & Yao, Y. D. Evidence for columnar organization in the auditory cortex of the mouse. *Hear. Res.* **137**, 174–177 (1999).
9. Blaschke, M. *et al.* A single amino-acid determines the subunit-specific spider toxin block of alpha-amino-3-hydroxy-5-methylisoxazole-4-propionate kainate receptor channels. *Proc. Natl. Acad. Sci. USA* **90**, 6528–6528 (1993).
10. Brackley, P. T., Bell, D. R., Choi, D. K., Nakanishi, K. & Usherwood, P. N. Selective antagonism of native and cloned kainate and NMDA receptors by polyamine-containing toxins. *J. Pharmacol. Exp. Ther.* **266**, 1573–1580 (1993).
11. Herlitze, S. *et al.* Argiotoxin detects molecular differences in AMPA receptor channels. *Neuron* **10**, 1131–1140 (1993).
12. Washburn, M. S. & Dingledine, R. Block of alpha-amino-3-hydroxy-5-methyl-4-isoxazolepropionic acid (AMPA) receptors by polyamines and polyamine toxins. *J. Pharmacol. Exp. Ther.* **278**, 669–678 (1996).
13. Toth, K., & McBain, C. J. Afferent specific innervation of two distinct AMPA receptor subtypes on single hippocampal interneurons. *Nat. Neurosci.* **1**, 572–578 (1998).
14. Dingledine, R., Borges, K., Bowie, D. & Traynelis, S. The glutamate receptor ion channels. *Pharmacol. Rev.* **51**, 7–61 (1999).
15. Markram, H., Lubke, J., Frotscher, M., Roth, A. & Sakmann, B. Physiology and anatomy of synaptic connections between thick tufted pyramidal neurones in the developing rat neocortex. *J. Physiol. (Lond.)* **500**, 409–440 (1997).
16. Faber, D. & Korn, H. Applicability of the coefficient of variation method for analyzing synaptic plasticity. *Biophys. J.* **60**, 1288–1291 (1991).
17. DeCharms, R. C., Blake, D. T. & Merzenich, M. M. Optimizing sound features for cortical neurons. *Science* **280**, 1439–1443 (1998).
18. DeCharms, R. C. & Zador, A. Neural representation and the cortical code. *Annu. Rev. Neurosci.* **23**, 613–647 (2000).
19. Kilgard, M. P. & Merzenich, M. M. Plasticity of temporal information processing in the primary auditory cortex. *Nat. Neurosci.* **1**, 727–731 (1998).
20. Zucker, R. S. Short-term synaptic plasticity. *Annu. Rev. Neurosci.* **12**, 13–31 (1989).
21. Zucker, R. S. Calcium- and activity-dependent synaptic plasticity. *Curr. Opin. Neurobiol.* **9**, 305–313 (1999).
22. Debanne, D., Guerineau, N. C., Gahwiler, B. H. & Thompson, S. M. Paired pulse facilitation and depression at unitary synapses in rat hippocampus: quantal fluctuation affects subsequent release. *J. Physiol. (Lond.)* **491**, 163–176 (1996).
23. Feldman, D. E. Timing-based LTP and LTD at vertical inputs to Layer II/III pyramidal cells in rat barrel cortex. *Neuron* **27**, 45–56 (2000).
24. Schreiner, C. E., Read, H. L. & Sutter, M. L. Modular organization of frequency integration in primary auditory cortex. *Annu. Rev. Neurosci.* **23**, 501–529 (2000).
25. Abbott, L. F., Varela, J. A., Sen, K. & Nelson, S. B. Synaptic depression and control of cortical gain. *Science* **275**, 220–224 (1997).
26. Giraud, A. *et al.* Representation of the temporal envelope sounds in the human brain. *J. Neurophysiol.* **22**, 1588–1598 (2000).
27. Kaas, J. & Hackett, T. 'What' and 'where' processing in the auditory cortex. *Nat. Neurosci.* **2**, 1045–1047 (1999).